Magnetic Resonance Microscopy of Collagen Mineralization

Ingrid E. Chesnick,* Jeffrey T. Mason,* Anthony A. Giuseppetti,† Naomi Eidelman,† and Kimberlee Potter*
*Department of Biophysics, Armed Forces Institute of Pathology Annex, Rockville, Maryland; and †Paffenbarger Research Center, American Dental Association Foundation, National Institute of Standards and Technology, Gaithersburg, Maryland

ABSTRACT A model mineralizing system was subjected to magnetic resonance microscopy to investigate how water proton transverse (T_2) relaxation times and magnetization transfer ratios can be applied to monitor collagen mineralization. In our model system, a collagen sponge was mineralized with polymer-stabilized amorphous calcium carbonate. The lower hydration and water proton T_2 values of collagen sponges during the initial mineralization phase were attributed to the replacement of the water within the collagen fibrils by amorphous calcium carbonate. The significant reduction in T_2 values by day 6 ($p < 0.001$) was attributed to the appearance of mineral crystallites, which were also detected by x-ray diffraction and scanning electron microscopy. In the second phase, between days 6 and 13, magnetic resonance microscopy properties appear to plateau as amorphous calcium carbonate droplets began to coalesce within the intrafibrillar space of collagen. In the third phase, after day 15, the amorphous mineral phase crystallized, resulting in a reduction in the absolute intensity of the collagen diffraction pattern. We speculate that magnetization transfer ratio values for collagen sponges, with similar collagen contents, increased from 0.25 ± 0.02 for control strips to a maximum value of 0.31 ± 0.04 at day 15 ($p = 0.03$) because mineral crystals greatly reduce the mobility of the collagen fibrils.

INTRODUCTION

The study of mineralized collagen by conventional techniques, such as x-ray or neutron diffraction, has yielded little information about subtle changes to the collagen matrix that might occur during the mineralization process. Many reports have focused on the effect of drying or demineralization on the collagen lateral packing (1–5), or the effect of different mineral densities, from different tissue sources, on the collagen fiber *d*-spacing (6). Alternatively, scanning electron microscopy (SEM) and transmission electron microscopy have been used to study the arrangement of mineral crystals around collagen molecules (7–10); however, such studies demand that mineralized specimens be exposed to various preparative solvents that can alter the natural spacing of the collagen fibrils. In this work we propose to study a model system in which a collagen sponge is mineralized with calcium carbonate, using magnetic resonance microscopy (MRM). This noninvasive imaging modality is capable of generating parametric maps of water proton transverse (T_2) relaxation times and magnetization transfer ratios (MTRs), which can be used to monitor the state of mineral and collagen, respectively.

Water proton T_2 values are highly dependent on molecular motion; thus, when water molecules become immobilized through ionic or dipolar interactions at the surface of a mineral, the T_2 of the surrounding solution is reduced because of fast exchange processes with the mineral-bound water molecules (11,12). In the presence of mineral deposits with a bulk magnetic susceptibility different from that of water, T_2 relaxation times are further reduced due to heterogeneities in the local magnetic field, and can therefore provide a measure of the mineral content of the sponge. With x-ray-based techniques, this may be difficult to achieve because of the relatively low mineral content. This is particularly the case if the mineral is amorphous, which broadens the diffraction peaks and reduces the ability to resolve them.

Alternatively, one can assess the collagen component of this model by measuring the MTR of surrounding water protons. Typically, macromolecular spins exhibit a much broader absorption line shape than mobile water protons and can be selectively saturated by the application of an off-resonance pulse before a standard imaging sequence (13,14). Saturated macromolecular spins exchange with mobile water protons, resulting in a reduction in the detected signal compared to a sequence without an off-resonance saturation pulse. The amount of signal loss is dependent on the exchange processes that take place within the tissue, and can be used to identify unique tissue components. For example, it is widely accepted that collagen-containing tissues give rise to a significant MT effect, which is the result of cross-relaxation between mobile water protons and hydroxyl groups on the hydroxyproline residues of collagen (13,14). Notably, calibration curves of MTR and collagen content have been derived for articular cartilage (15), engineered cartilage (16), and collagen gels (15,17,18). In our experience, collagen in mineralizing tissues, such as the avian growth plate (19), calcifying cartilage (20), and osteoblast-seeded polymer scaffolds (21), gives rise to a significant MT effect. More importantly, in zones where mineral deposits are localized, the MT effect is enhanced compared to that in surrounding unmineralized tissue (22). However, as the mineral content

Submitted August 30, 2007, and accepted for publication April 21, 2008.

Address reprint requests to Kimberlee Potter, PhD, Dept. of Biophysics, Armed Forces Institute of Pathology Annex, 1413 Research Blvd., Rockville, MD 20850. Tel.: 301-319-0208; Fax: 301-319-0638; E-mail: potterk@afip.osd.mil.

Editor: Arthur G. Palmer 3rd.

0006-3495/08/08/2017/10 $2.00

doi: 10.1529/biophysj.107.120923

approaches that of mature bone, the T_2 of the water protons in the bone is markedly reduced and thus the MT effect cannot be measured accurately. We expect that the measured MT effect before mineralization reflects the collagen content of the mineralizing osteoid tissue. We speculate that during bone formation, the MT effect is enhanced due to an increase in the collagen content of the mineralized zone, brought about by formation of mineral between the collagen fibrils and the correlated reduction in the intermolecular spacing of the collagen fibrils (23). The collagen fibrils pack together more tightly, resulting in a higher volume density of collagen and thus higher MTR values.

To characterize the changes we have observed for bone (19–22), we subjected a model mineralizing system to MRM. In this model system, calcium carbonate mineral is produced when an aqueous solution of calcium chloride is exposed to the decomposition products of ammonium carbonate. In the presence of a charged polypeptide additive, such as poly(acrylic acid) or poly(aspartic acid), calcium carbonate is formed as a liquid-droplet mineral precursor phase (24). This polymer-induced liquid-precursor (PILP) is drawn into the gaps and grooves of collagen fibrils by capillary action, and upon solidification forms plate-like crystals within the collagen fibrils reminiscent of those observed for normal bone (25–27). The formation of intrafibrillar mineral deposits has been confirmed by selected area diffraction of the center of a mineralized collagen fiber (27). In the absence of poly(acrylic acid), rhombohedral crystals of calcite form on the surface of the collagen fibers (26,27). To confirm that we were able to reproduce the model mineralizing system described in the literature (25–27), we subjected our model system to SEM. The advantage of this model system is that the quantity of collagen is unchanged, so observed changes in the measured MT effect can be attributed to changes to the collagen fibrils induced by the mineral deposits.

The lateral spacing or equatorial diffraction spacing of collagen derived by x-ray diffraction has been used to confirm the lateral collapse of the collagen present in mineralized turkey leg tendon compared to unmineralized tendon (1,4). Therefore, we attempted to assess changes in the lateral packing arrangement of collagen during the mineralization process by using x-ray diffraction to examine collagen sponges mineralized under PILP conditions. If the behavior of water protons reported by MRM can be related to molecular level changes to the collagen fibrils due to mineral deposition, it is our expectation that the MRM experiment can be used to gain important insights into the mineralizing process in vivo.

MATERIALS AND METHODS

Mineralization of collagen sponges

Details of the PILP process are described elsewhere (25–27). Briefly, a Cellagen (reconstituted Type I collagen) sponge (ICN Biomedicals, Aurora, OH) was cut into rectangular strips (2 mm × 10 mm × 1 mm), and eight strips were prepared for each time point. Before mineralization, the collagen strips were rehydrated in 12 mM calcium (II) chloride dihydrate ($CaCl_2.2H_2O$; Sigma-Aldrich, St. Louis, MO) at 4°C for 3 days. At the start of the mineralization process, four strips were placed in a petri dish (diameter = 35 mm; Corning, Corning, NY) containing 1.5 mL of 24 mM $CaCl_2$, 1 mL of 1 mg/mL polyacrylic acid (PAA, poly (acrylic acid, sodium salt), M_w = 5100; Sigma-Aldrich), and 0.5 mL of deionized water, for a final concentration of 12 mM $CaCl_2$ and 0.33 mg/mL PAA. Two petri dishes containing four strips each were used for each time point. Before use, all solutions were filter-sterilized using a benchtop filter flask (Corning) with a 0.22-μm filter. The dishes were sealed with Parafilm and three pinholes were introduced in the film to allow for the exchange of gases. Dishes were transferred to a dessicator with three vials containing 3 g crushed ammonium carbonate (Sigma-Aldrich) each. The vials were sealed with Parafilm and a single pinhole was made in the film to allow the diffusion of ammonia and carbon dioxide. The dessicator was evacuated and stored at 4°C. Every 3 days the calcifying solution for the existing dishes was changed and additional dishes were added to the chamber. This process was repeated until 24 days had passed. In addition to experimental samples, a control dish was included with each series. The control dish contained the same calcifying solution as the experimental samples (12 mM $CaCl_2$ and 0.33 mg/mL PAA), but the strips were not exposed to the ammonium carbonate.

At the end of 24 days, all of the samples were removed from the desiccator, rinsed twice in 12 mM $CaCl_2$ to remove any residual PAA, and stored in dishes containing 12 mM $CaCl_2$ at 4°C. MRM was performed on at least three sets of samples containing strips for the different time points. After MRM, at least two specimens from each time point were analyzed by x-ray diffraction. One set of strips was used for SEM analysis (see below). The remaining specimens were subjected to a biochemical assay for calcium.

Biochemical assay for calcium

Each collagen strip was washed with deionized water to remove residual calcium chloride before the assay. The details of this Alizarin red-based calcium assay have been published elsewhere (28). Briefly, each sample was placed in a 1.5 mL Eppendorf tube to which was added 250 μL of a 40 mM aqueous solution of Alizarin red S (Sigma-Aldrich). The samples were incubated with shaking for 20 min at room temperature. After the incubation period, excess Alizarin red dye was removed and the samples were washed with 1 mL of deionized water for 5 min. This step was repeated to remove excess dye from the sample. Excess water was removed, 800 μL of 10% v/v acetic acid (Sigma-Aldrich) was added to each tube, and the samples were incubated for 30 min at room temperature. After the incubation period the samples were vortexed for 30 s and overlaid with 500 μL of light mineral oil (Sigma-Aldrich). They were then incubated for 10 min at 85°C to solubilize the Alizarin red-calcium complex. The samples were cooled on ice for 10 min and then centrifuged at 11,500 × g for 15 min. After centrifugation, 500 μL of the sample solution below the mineral oil was transferred to a clean 1.5 mL Eppendorf tube and the pH of the solution was adjusted to between 4.1 and 4.5 with 10% v/v ammonium hydroxide (Sigma-Aldrich) if required. Then 10 μL of the sample were aliquoted in triplicate into a 96-well plate (Corning) containing 140 μL of pH 4.2-ammonium acetate solution. Varying concentrations of Alizarin red solution diluted in the same ammonium acetate solution were used as standards and the ammonium acetate solution was used as the blank. The plate was read at 405 nm on a SpectraMax M5 microplate reader (Molecular Devices, Sunnyvale, CA). For this assay, the calcium content of each sample was calculated with SoftMax Pro 4.8 software (Molecular Devices), using a 1:1 stoichiometric ratio for the Alizarin red-calcium complex (29).

Magnetic resonance microscopy

Collagen strips for each time point (3, 6, 9, 13, 15, 18, and 24 days) along with control strips were analyzed by MRM. For the MRM experiment, strips were sandwiched between two glass slides (width = 12 mm, height = 75 mm)

with rubber spacers (~1 mm thick) located near the top and bottom edges of the glass slide. The spacers were used to immobilize the collagen strips and to prevent the strips from becoming crushed. The glass slides were placed in a glass tube (outer diameter = 15 mm) containing 4 mL of 12 mM $CaCl_2$ solution. The sample was degassed under vacuum and heated to 37°C for 2 h to remove air bubbles introduced during the preparation of the sample for MRM.

MRM experiments were performed on a Bruker DMX spectrometer (Bruker Biospin MRI, Billerica, MA) coupled to a wide-bore magnet operating at 9.4 T (400 MHz for ^{1}H) equipped with a microimaging gradient accessory. All samples were imaged at 37°C. MRM images of the collagen strips had a field of view of 30 mm × 15 mm, a matrix size of 256 × 128, a nominal in-plane resolution of 117 μm, and a slice thickness of 1.8 mm. The imaging slice was aligned with the space between the two glass slides and the slice thickness was set to be greater than the gap between the two glass slides containing the collagen strips, but less than the total thickness of the two glass slides. Thus, the MRM signal can be attributed to protons between the two glass slides and not from the surrounding solution. The following MRM parameters were evaluated spatially: the water proton density (PD), the water proton transverse (T_2) relaxation time, and the MTR.

Quantitative T_2 relaxation maps were calculated on a pixel-by-pixel basis from 16 images acquired with a multiecho sequence (repetition time [TR] = 5 s, echo time [TE] = 10–160 ms). Images were fit on a pixel-by-pixel basis with a single exponential decay function of the form: $I = I_0 \exp(-\mathrm{TE}/T_2) +$ offset, where I_0 is the water PD, T_2 is the transverse relaxation time to be determined, and the offset is the noise level in the image. The PD values extracted by this calculation provide a direct measure of the number of water protons present in each pixel in the image. The PD values for the collagen strips were normalized to the PD value of the solution contained between the two slides to yield the hydration state of each strip.

The MTR value at each pixel was calculated from a series of images acquired with a 12 μT saturation pulse applied 6000 Hz off-resonance, with varying saturation times (t_p = 0.2–5 s), before a standard spin-echo imaging sequence (30). The observed image intensity, $M_s(t_p)$, after the application of a saturation pulse of length t_p was fit according to the expression $M_s(t_p) = (M_o - M_{so}) \exp(-t_p/T_{1sat}) + M_{so}$, where M_{so} and M_o are the image intensities acquired with and without, respectively, the application of an infinitely long saturation pulse, and T_{1sat} is defined as the longitudinal relaxation time of the free protons in the presence of an off-resonance saturation pulse. The MTR map was then calculated using the equation $[1 - (M_{so}/M_o)]$. The MTR parameter provided a measure of the rate of transfer of magnetization from mobile water protons to protons on large immobile macromolecules like collagen. All image analysis was performed using Bruker Paravision software as well as user-defined procedures in IDL (Interactive Data Language; ITT Visual Information Solutions, Boulder, CO). Regions of interest (ROIs) were identified on PD, T_2, and MTR maps of the PILP samples, and the MRM values of the pixels within each ROI were averaged together. The PD, T_2, and MTR values reported for each time point represent the average of at least three strips (for day 24) to as many as nine strips (for the controls) from at least three different PILP experiments.

MRM measurements were subjected to pairwise multiple comparisons with a Bonferroni t-test and significance was determined at $p < 0.05$. For the MTR data, PILP exposure times were compared with controls to achieve statistical significance. All statistical tests were performed using SigmaStat Version 3.5 (Systat Software, Point Richmond, CA).

X-ray diffraction

X-ray diffraction measurements were performed with a Bruker powder diffractometer equipped with an 11.5-cm-diameter xenon-gas-filled HiStar area detector (Bruker-AXS, Madison, WI). The PILP samples were placed in 2.5-mm borosilicate glass capillaries (Charles Supper Co., Natick, MA) and hydrated with 12 mM $CaCl_2$ solution. Acid-washed glass beads (diameter ≤ 160 μm; Sigma) were used to situate the sample at the correct height in the sample tube. The capillaries were then flame-sealed and placed in a custom-made capillary holder consisting of a microchuck (0.5–4 mm adjustment range) attached to a three-axis goniometer head. The capillaries were centered in the x-ray beam path using the optical microscope of the goniometer stage. The x-ray source was a copper anode long fine-focus sealed tube operated at 1.5 kW. A flat graphite monochromator was used to separate the Kα radiation from the white light spectrum. The emission from the monochromator was collimated by means of a 500-μm pinhole tube. The area detector was placed on the 2θ arm of the goniometer stage at a distance of 26.6 cm from the sample. The exact sample-to-detector distance and beam center were calibrated with a silver behenate standard for the low-angle region (2θ = 0–30°) and an aluminum oxide (corundum) standard for the wide-angle region (2θ = 30–70°), where 2θ is the diffraction angle. Before data collection, the area detector was calibrated using a ^{55}Fe source to adjust the detector bias, measure the detector background, and determine the fiducial correction for the detector. Sample temperature was regulated with a temperature-controlled nitrogen stream (5 L/min) from a Cryostream model 600 cooler (Oxford Cryosystems, Oxford, UK). The gas discharge tip of the cooler was placed 5 mm from the point of intersection of the x-ray beam with the capillary tube. All samples were measured at 24 ± 0.2°C.

Diffraction data from the PILP samples were collected and displayed in real time as a 1024 × 1024 data frame collected from the HiStar area detector. Collection times of 1 h were used for all samples, which corresponds to ~10 million cumulative counts in the area detector data frame. Diffraction data were collected over a 2θ angle of 0–70°. The data frames, which consist of the Debye-Scherrer diffraction rings arising from the PILP samples, were analyzed to produce a file of relative diffraction intensities versus the 2θ angle using the General Area Detector Diffraction Software (GADDS) supplied by Bruker. These files were imported into GRAMS/AI version 7 (Thermo Galactic, Salem, NH) for data analysis. Deconvolution (peak fitting) was used to separate the diffraction peaks arising from the collagen sponge and the mineral calcite. Peak areas were determined by integration of the deconvoluted peaks, and peak positions were assigned as the center of mass of the upper one-third of the peaks based on peak height. Plots of diffraction profiles and their derived parameters were created using Origin graphing software, version 7 (OriginLab, Northampton, MA).

Scanning electron microscopy

Collagen strips were washed with distilled water to remove residual calcium chloride and then air-dried for 24 h. The dried strips were cut into three sections. Sections from each time point were mounted on an SEM stub, sputter-coated with gold (Desk II; Denton Vacuum, Moorestown, NJ), and examined with a scanning electron microscope (model JSM-5300; JEOL, Peabody, MA). Images with magnifications of ×50, ×150, ×1000, ×5000, and ×10000 were obtained. One section of the 18-day sponge was etched with 0.1 M HCl (Ricca Chemical Co., Arlington, TX) for 15 min to remove excess surface mineral, and one section was bleached with 0.5 vol% NaOCl (Ultra Clorox; Clorox Professional Products, Oakland, CA) for 15 min to remove the organic matrix. Acid-treated and bleach-treated sections were air-dried and examined with SEM as described above.

RESULTS

After exposure to PILP conditions, collagen strips were sandwiched between two glass slides and stored in a solution of calcium chloride before the MRM experiment. A representative sample, shown in Fig. 1, contains six collagen strips exposed to PILP conditions for 18, 15, 13, 9, 6, and 3 days, moving from the top to the bottom of the stack with a control strip, located at the bottom of the stack. Controls were included in each experiment so that samples taken at different exposure times could be readily compared with a collagen strip with no mineral deposits. The control strip was almost

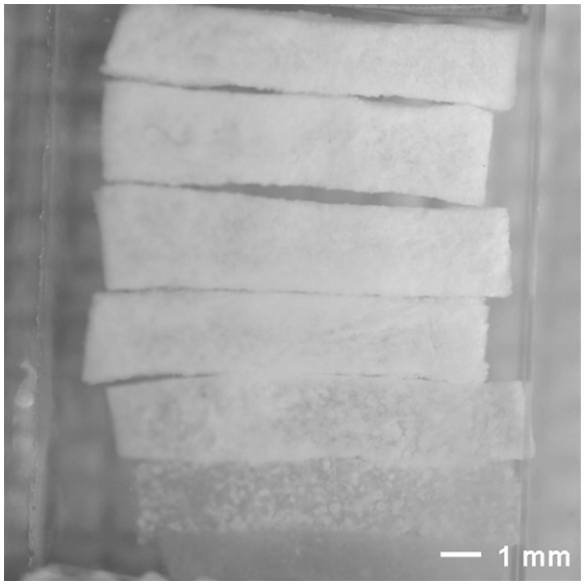

FIGURE 1 Photograph of a stack of collagen strips from a single PILP experiment. At the bottom of the stack was a control strip that was not exposed to PILP conditions. Adjacent to the control were collagen strips exposed to PILP conditions for 3, 6, 9, 13, 15, and 18 days (from *bottom* to *top*). Strips were imaged between two glass slides separated by a spacer. Initially the collagen strips were translucent, but they became more opaque with longer exposure times to PILP conditions. (Bar = 1 mm.)

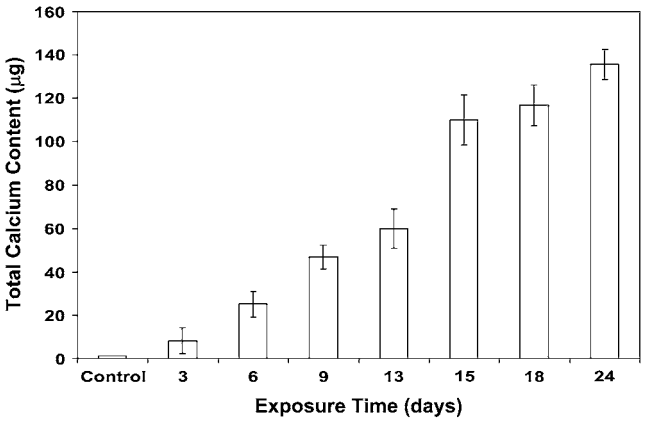

FIGURE 2 Total calcium content of collagen strips plotted against the exposure time to PILP conditions. The calcium content was determined using an Alizarin red dye binding assay and each error bar represents the data from five collagen strips.

translucent owing to a lack of mineral, whereas the strips for the later time points (15 and 18 days) were opaque as a result of profuse mineral deposits throughout the samples. At short exposure times (3 and 6 days), individual clusters of early mineral deposits were clearly visible.

Collagen strips from the early time points would collapse under their own weight once removed from solution. This did not occur with strips from the later time points because the mineral content in these strips was enough to impart rigidity to the sponge-like structure. We did not measure the mechanical properties of the individual strips, but we did measure their total calcium content using an Alizarin red dye-binding assay (28). These results are summarized in Fig. 2. We found that there was a small amount of residual calcium in our controls and that the calcium content of the strips increased almost linearly with increasing exposure times to PILP conditions. In this particular run, the calcium content increased dramatically from day 13 to day 15 ($p < 0.001$). In separate experimental runs this transition occurred as early as day 6 (data not shown). Thereafter, the calcium content increased slightly between day 15 and day 24. In this graph, each time point represents the average of three replicate measurements for five strips taken from roughly the same location in the Cellagen sponge and cut to approximately the same size.

Representative MRM images of the strips shown in Fig. 1 are presented in Fig. 3. PD (Fig. 3 *A*) and T_2 (Fig. 3 *B*) maps yield information about the presence or absence of mineral deposits, whereas the MTR map (Fig. 3 *C*) yields information about the state of constituent collagen fibrils. The control strip at the bottom of the stack had the highest signal intensity in the PD and T_2 maps and the lowest signal intensity in the MTR map. The two strips at the top of the stack, which were exposed to PILP conditions for 15 and 18 days, had the lowest signal intensity in the PD and T_2 maps and the highest signal intensity in the MTR maps. The transition from a low-mineral-density strip to high-mineral-density strip is readily apparent in the MRM maps presented. These MRM images, unlike SEM images, are not restricted to the surface of the sponge, but provide spatial maps of the distribution of mineral and collagen throughout each individual strip. Strips from the later time points appear to be uniformly mineralized, whereas those for the early time points have localized zones of high mineral density; see for example the hypermineralized zone in the day 6 strip (third from the bottom) in Fig. 3.

To better illustrate how water proton MRM properties change with the onset of mineralization, the MRM properties of collagen strips exposed to PILP conditions for increasing periods of time are summarized in Fig. 4. Each exposure time represents MRM data averaged for at least three strips (for day 24) to as many as nine strips (for controls) from at least three separate experimental runs. The hydration state (Fig. 4 *A*) and the water proton T_2 relaxation time (Fig. 4 *B*) of the collagen strips decreased with increasing exposure times. The appearance of the small mineral deposits resulted in significant reductions in both the hydration state ($p < 0.001$) and T_2 values ($p < 0.001$) by day 6 compared to controls. There were marked reductions in collagen sponge hydration between days 3 and 9 ($p = 0.008$) and days 9 and 18 ($p < 0.001$). T_2 values were similarly reduced between days 3 and 6 ($p < 0.01$) and days 9 and 15 ($p < 0.001$).

Conversely, MTR values measured for collagen strips as a function of exposure time increased from 0.25 ± 0.02 for

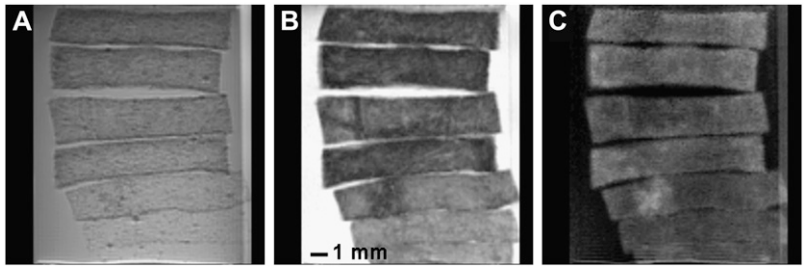

FIGURE 3 Quantitative PD (*A*), T_2 (*B*), and MTR (*C*) maps acquired for the stack of collagen strips shown in Fig. 1. Adjacent to the control strip at the bottom of the stack were collagen strips exposed to PILP conditions for 3, 6, 9, 13, 15, and 18 days (from *bottom* to *top*). MRM images were acquired at 37°C with a nominal in-plane resolution of 117 μm and slice thickness of 1.8 mm (*bar* = 1 mm). Bright (dark) regions on PD and T_2 maps correspond to regions with high (low) hydration and low (high) mineral content. Bright (dark) regions on MTR maps correspond to regions with more (less) mineral-encapsulated collagen.

control strips to a maximum value of 0.31 ± 0.04 at day 15 and then decreased to 0.29 ± 0.03 by day 24. MTR values changed very gradually over the observation period and the values measured at days 13 and 15 were significantly higher ($p = 0.04$ and $p = 0.03$, respectively) compared to controls. Notably, the error in the MTR values measured for all days was larger than the error for the control group.

After the MRM measurements, hydrated collagen strips were subjected to x-ray powder diffraction analysis. Diffraction data were collected over a 2θ diffraction angle of 0–70°. X-ray diffraction profiles for collagen strips exposed to PILP conditions for 3, 6, 9, 13, 15, 18, and 24 days are presented in Fig. 5 together with a diffraction profile of a control strip with no mineral deposits. Each diffraction profile represents the average of five measurements made at different locations within a single collagen strip. The diffraction profile for the control strip was identical to that of fully hydrated Type I collagen (Sigma-Aldrich) derived from rat tail collagen (data not shown), indicating that the texture of the Cellagen sponge did not alter the normal Type I collagen diffraction scattering. The collagen diffraction profile consisted of a discrete equatorial diffraction series, which arises from the axial crystalline-like lateral packing interactions of the tropocollagen molecules (31). The diffraction lines from this quasi-hexagonal lattice were superimposed on a continuous diffuse scattering profile that is believed to arise from lateral packing disorder in the gap regions of the fibrils (32). In this study, a collagen diffraction peak was observed at 10.607°, corresponding to a lateral molecular spacing of

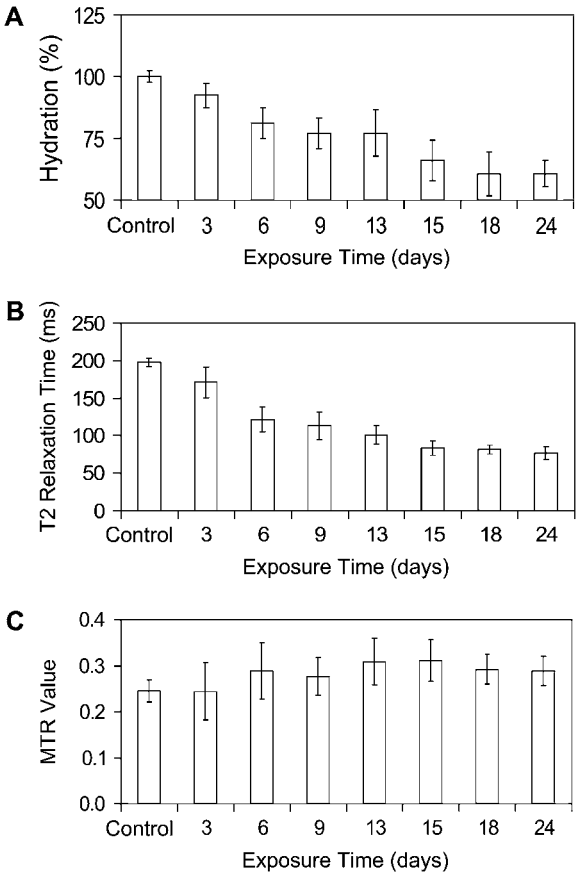

FIGURE 4 MRM graphs of the hydration state (*A*), T_2 relaxation time (*B*), and MTR value (*C*) of collagen strips exposed to PILP conditions for varying lengths of time. Data extracted from MRM images are presented with data for control strips for comparison purposes. Each error bar represents a minimum of three samples (for day 24) and a maximum of nine samples (for the controls).

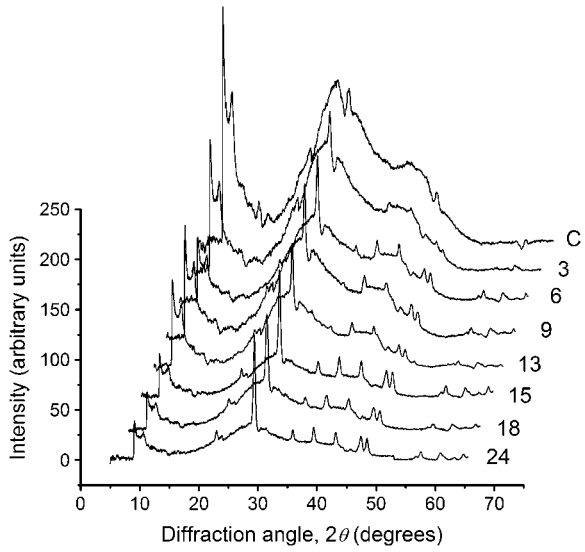

FIGURE 5 X-ray diffraction profiles acquired for representative samples of collagen strips exposed to PILP conditions for 3, 6, 9, 13, 15, 18, and 24 days. The incubation time is indicated adjacent to each profile. The diffraction profile of a control strip (labeled *C*) is shown for comparison purposes. Each diffraction profile represents the average of five measurements made at different locations within the same strip.

1.67 nm, and this observed lateral spacing was constant over the 24-day incubation period.

Exposure to PILP conditions resulted in the formation of a crystalline mineral phase, with diffraction peaks observed between 29° and 66° (Fig. 5). These peaks were seen to grow in intensity, becoming progressively more prominent and slightly narrower, throughout the 24-day incubation period. Interestingly, both the sharp (10.607°) and diffuse (~29°) collagen peaks appeared to decrease in intensity concomitant with the increase in intensity of the mineral peaks. The mineral peak positions remained essentially invariant throughout the 24-day incubation under PILP conditions. The intense peak at ~29°, which corresponds to the (104) plane of calcite, shifted only slightly from 29.367° (day 3) to 29.382° (day 24). The mineral peaks indexed to those of a calcite ($CaCO_3$) standard (registry number 05-0586) from the Powder Diffraction File (PDF) database (International Center for Diffraction Data, Newton Square, PA). In fact, 14 of the 17 peaks of the calcite standard were identified in the PILP specimens, with the average deviation between the standard and the sample peak positions being ±0.186°. The three calcite standard peaks that were not seen in the PILP specimens were minor peaks, with relative peak intensities below 5%, which were likely buried below the collagen diffuse scattering profile. The calcite diffraction peaks became sharper with incubation time under PILP conditions. For example, the form factor (ratio of height to width) of the peak at ~29° increased from 2.41 (day 3) to 2.66 (day 24).

In Fig. 6 the mineral content of the collagen strips, expressed as the percent crystalline mineral, is plotted as a function of exposure time to PILP conditions. The percent crystalline mineral content for each strip was estimated by summing the areas of all of the calcite diffraction peaks and expressing this value as a percentage of the total area of the diffraction profile shown in Fig. 5. The connecting lines in Fig. 6 were drawn to show the trend in the data. The crystalline mineral content measured by x-ray diffraction increased dramatically between days 13 and 15, which is consistent with the observed change in the biochemically determined calcium content for mineralizing collagen strips from the same experimental run shown in Fig. 2.

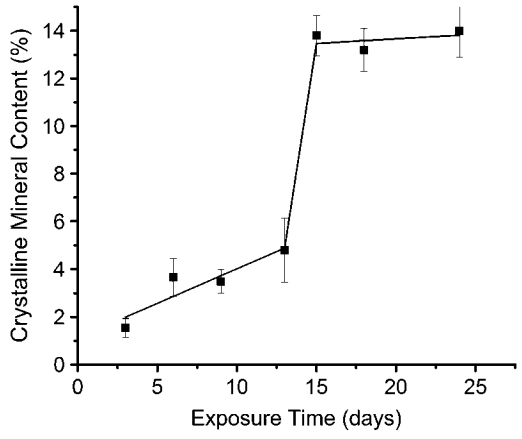

FIGURE 6 Percent crystalline mineral in the collagen strips is plotted as a function of exposure time to PILP conditions. The percent crystalline mineral content was estimated by summing the areas of all of the calcite diffraction peaks and expressing this value as a percentage of the total area of the diffraction profile shown in Fig. 5. The largest change in crystalline mineral content was observed to occur between days 13 and 15. The connecting lines in the figure were drawn to show the trend in the data.

To confirm that the PILP experiment was conducted successfully, and to explain the observed MRM and x-ray diffraction results, we subjected a series of collagen sponges to SEM analysis. In Fig. 7, representative SEM images of an unmineralized collagen control sponge (*A* and *G*) are presented together with SEM images of PILP samples from days 3 (*B* and *H*), 9 (*C* and *I*), 13 (*D* and *J*), 15 (*E* and *K*), and 18 (*F* and *L*). The unmineralized collagen sponge in Fig. 7 *A* appears relatively flat with some underlying texture, which was attributed to randomly oriented collagen fibers seen in Fig. 7 *G*, acquired at higher magnification. On day 3, isolated islands of mineral deposits (*black arrows*) were observed on the surface of the collagen sponge (Fig. 7 *B*). Individual mineral islands, observed at higher magnification, revealed calcite disks oriented perpendicular to the long axis of the collagen fibers in an essentially periodic banding pattern (Fig. 7 *H*). At longer exposure times, the number of mineral islands increased (see the SEM image of the day-9 sponge in Fig. 7 *C*). Additionally, collagen fibers within the mineral islands of the day-9 sponge were completely encapsulated by mineral (Fig. 7 *I*). By day 13, the surface of the sponge was covered by numerous mineral islands (Fig. 7 *D*), with some unmineralized collagen fibers between the mineral islands (indicated by *white arrows* in Fig. 7 *J*). By days 15 and 18, the intervening space between mineral islands was filled with mineral (see Fig. 7, *E* and *F*, respectively). In the corresponding high-resolution SEM image of the day-15 sponge (Fig. 7 *K*), the collagen appeared matted owing to the presence of the mineral in the gaps and grooves between mineralized collagen fibers. At day 18, however, some unmineralized collagen fibers were still evident in the underlying layers (Fig. 7 *L*). Note that the diameter of the mineralized fibrils at all times as seen in the high magnification images is ~4–5 times that of the control fibrils.

The SEM images in Fig. 8 correspond to an unmineralized collagen sponge (*A*) together with untreated (*B*), acid-etched (*C*), and bleach-treated (*D*) sections from the same 18-day specimen. Careful etching of the 18-day specimen with 0.1 M HCl to remove excess surface mineral deposits revealed mineral-encapsulated collagen fibers (Fig. 8 *C*). Treatment with bleach removed unmineralized collagen fibers as well as those fibers exposed by microcracks formed during the drying process. This treatment confirmed that the mineral deposits are colocalized with the collagen fibers and that residual calcite disks appear oriented perpendicular to the long axis of collagen fiber (Fig. 8 *D*).

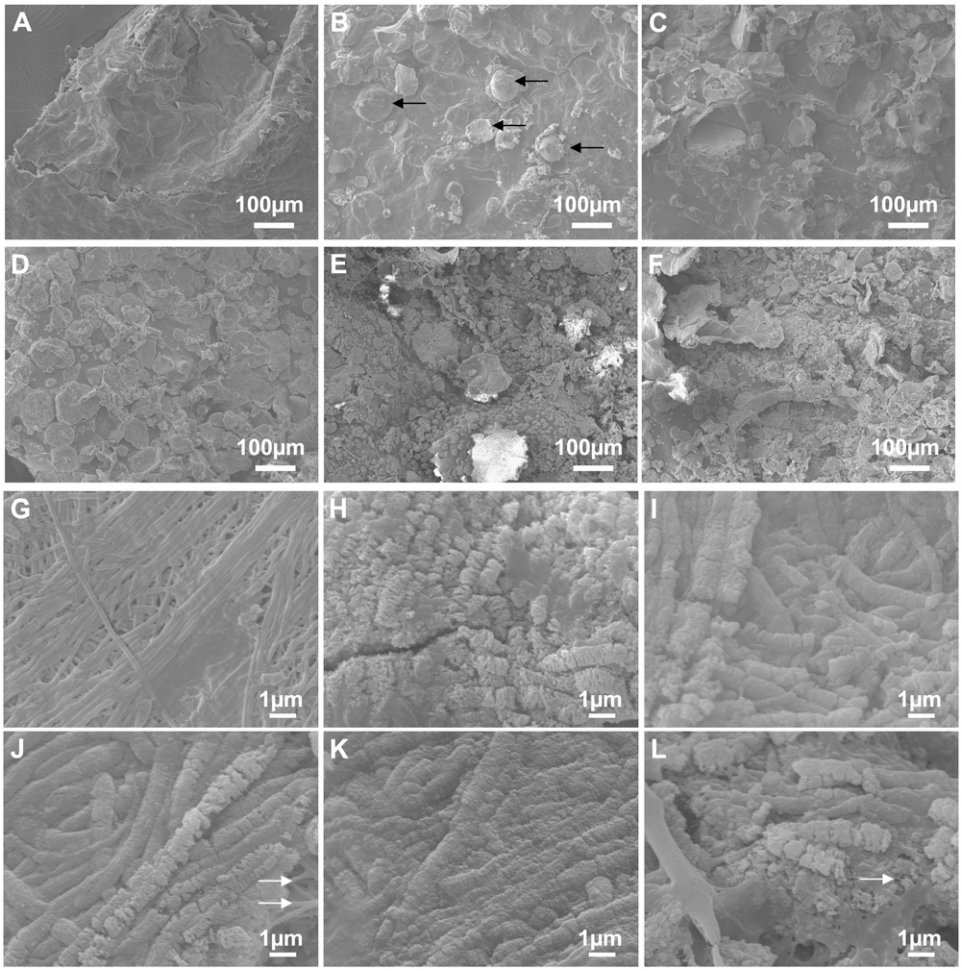

FIGURE 7 Representative SEM images of an unmineralized control collagen sponge (*A* and *G*) are presented together with SEM images of PILP samples from days 3 (*B* and *H*), 9 (*C* and *I*), 13 (*D* and *J*), 15 (*E* and *K*), and 18 (*F* and *L*) taken at low (×150) and high (×10,000) magnification. Low-magnification images (*A–F*) reveal the gradual appearance of mineral nucleation sites or mineral islands, which become more numerous with increasing exposure time to PILP conditions. By day 15 much of the intervening space between the mineral islands is filled in with mineral. The higher-magnification SEM images (*G* and *H*), focused on individual mineral islands, reveal that mineral deposits are colocalized with collagen and the mineral occurs as calcite disks oriented perpendicular to the *c* axis of the collagen fibril in a roughly periodic arrangement. At longer exposure times to PILP conditions, the collagen fibrils at the surface of the sponge appear completely encapsulated by mineral. By day 15 many of the gaps and grooves between fibrils have been filled in with mineral, giving the collagen a matted appearance. By day 18, however, there were some unmineralized collagen fibrils evident in the underlying layers. Black arrows indicate mineral islands, and white arrows indicate unmineralized collagen fibrils.

DISCUSSION

The exact sequence of events that occurs during the PILP process is not completely understood. It is speculated that the acidic polymer phase separates to form small liquid-filled droplets in which amorphous calcium carbonate is stabilized (24–27). These droplets are then thought to adsorb to the fibrils and get pulled into the gaps and grooves of the fibrils by capillary action, forming calcite crystals that retain their fluidic shape (25–27). Similar studies have revealed how calcium carbonate can be molded into exquisite shapes, reminiscent of structures produced by invertebrates, using macroporous hydrogels (33). The mineralized deposits seen on SEM images of our PILP samples were comparable to those reported previously (25–27), which confirms that the PILP experiment was conducted successfully. However, the kinetics of droplet formation and the concentration of dissolved species are difficult to control by the vapor diffusion technique (24). This explains why the jump in calcium content, based on the results of our calcium assay for several experimental runs, varied between days 6 and 13. The observed variability within a single experimental run was attributed to the vapor diffusion technique, the variability in the size of each collagen strip, and the intrinsic heterogeneity of the Cellagen sponge.

The calcium content of the collagen sponges, measured with our calcium assay, resembles the percent crystalline mineral within the sponges, measured by x-ray diffraction. We speculate that much of the amorphous calcium carbonate (or PILP phase) is washed away during the washing stage of our calcium assay and only the calcium content of the insoluble calcite crystals is measured. The dramatic increase in the calcium content of the collagen sponges on day 15, measured biochemically, was attributed to a significant increase in the amount of crystalline mineral produced as the amorphous PILP phase crystallizes in the collagen fibrils. This result is consistent with the jump in the percent crystalline mineral deposits measured by x-ray diffraction at day 15. In addition, the observed reduction in the widths of the calcite diffraction peaks with increasing incubation time supports the increase in the microscopic order and crystallinity of the mineral phase as the amorphous mineral phase crystallizes. Intrafibrillar mineralization of the collagen fibers also explains the increase in the rigidity of the collagen net-

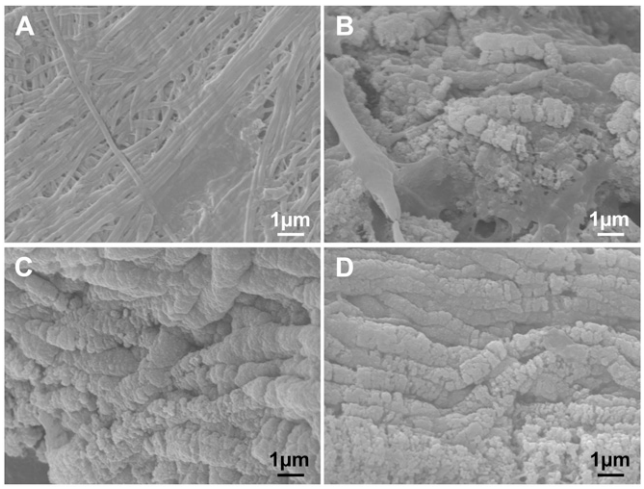

FIGURE 8 SEM images (×10,000) of unmineralized collagen sponge (*A*) together with untreated (*B*), acid-etched (*C*), and bleach-treated (*D*) 18-day specimens. Careful etching of the 18-day specimen with 0.1 M HCl removed excess surface mineral deposits and revealed mineral-encapsulated collagen fibrils. Treatment with bleach removed exposed collagen fibrils and confirmed that the mineral deposits are localized along collagen fibrils with calcite disks oriented perpendicular to the long axis of the fibrils.

work for sponges exposed to PILP conditions for longer than 15 days.

Despite its poor reproducibility, this model system provides the perfect opportunity to study the effect of mineral formation on the MRM properties of water protons within a collagen sponge in which the collagen content is not changing. This is not the case, however, with most mineralizing tissues. Here, both the hydration state and the water proton T_2 values were significantly reduced with the onset of mineralization. The reduced hydration state may be attributed to the displacement of water by the amorphous mineral phase. The reduction in water proton T_2 values with the appearance of crystalline mineral deposits may be attributed to the immobilization of water molecules, through ionic or dipolar interactions at the surface of the mineral, and to enhanced field heterogeneities caused by the different bulk magnetic susceptibility of the mineral from that of water. The results presented here are consistent with the findings from numerous studies concerned with understanding the effects of calcium salts on water proton MR relaxation times (11,12,34,35).

During the mineralization process the collagen content of the strips was expected to remain constant, and yet the water proton MTR values increased with exposure time to PILP conditions. Using a published calibration curve for MTR values versus collagen concentration measured under similar conditions (15), we found that during the PILP process the apparent collagen concentration increased from 2.6% w/v for controls to 3.5% w/v for samples from day 15. This apparent increase in collagen content, which cannot be a real increase in this constant collagen model system, could be an indirect effect of collagen consolidation during mineral formation. However, the results of our x-ray diffraction studies did not support the collapse of the Bragg-spacing for collagen with longer PILP exposure times. In this model system, we suspect that intrafibrillar mineralization, confirmed by our SEM studies, prevents the collapse of the collagen fibrils. We speculate that in this model system, higher MTR values are attributable to the increased rigidity of the collagen network due to intrafibrillar mineral deposition. This explanation is consistent with observed increases in MTR values with cross-link density at constant macromolecular concentrations for polyacrylamide gels (36), alginate gels (37), and formalin-fixed cartilage (38).

As stated above, the x-ray diffraction spacing for collagen remained constant at 1.67 nm throughout the PILP experiment. This result was in contrast to both neutron (39) and x-ray diffraction studies (1,5) in which it was determined that collagen equatorial diffraction spacing decreases as the mineral density of fully wet mineralized tissues increases. Specifically, Lees (23) established a linear correlation between the wet tissue density of collagen and the position of the diffraction peak at ~10.5°. Perhaps the reduction in the Bragg-spacing of collagen occurs only in mineralizing tissues, where hydroxyapatite is thought to form in the extrafibrillar space (7). Another reason for the lack of change in the diffraction spacing of collagen may lie in the heterogeneity of the mineralizing collagen sponge, which can lead to a measured x-ray intensity that is biased toward the mineral phase. The linear absorption coefficient (μ) is more than 10 times greater for minerals, such as calcite, than for organic molecules, such as collagen. Consequently, in a mixed phase containing both calcite and collagen, the mineral phase will scatter x rays to a much greater degree and will dominate the x-ray diffraction profile. This process, which is termed the absorptive effect (40), explains why on day 15, with the crystallization of the PILP phase, there was a dramatic reduction in the intensity of the collagen x-ray diffraction peaks and a marked increase in the intensities of the mineral x-ray diffraction peaks.

The observed collagen diffraction peaks, especially at the later time points, likely originate from regions within the collagen strip that have the lowest concentration of calcite crystals and/or contain mostly amorphous calcium carbonate. Although these areas are not expected to show significant changes in collagen fibril spacing, we expect the number of unmineralized collagen fibers to decrease with increasing exposure times to PILP conditions. The fact that we can still observe collagen diffraction peaks by day 24 supports the notion that some collagen fibers remain unmineralized. This result was confirmed by SEM and could be attributed to insufficient quantities of PILP to cover the entire surface of all the fibrils within the collagen sponge. Alternatively, mineralized deposits on the surface of the collagen sponge could dramatically reduce the infiltration of the PILP phase to the underlying layers, thereby hindering the complete mineralization of the sponge.

On further inspection of the MRM graphs in Fig. 4, we propose that the PILP process might be subdivided into three phases. In the first phase, between days 0 and 6, both the hydration state and the T_2 values are reduced compared to those of a control strip. This result may be attributed to the initial displacement of water from within the collagen fibrils by PILP droplets containing amorphous calcium carbonate, as well as the appearance of small mineral crystallites on the surface of the sponge. Notably, the diffraction peaks for calcite formed in the early PILP samples were much broader than those typically seen for macroscopic crystals, which indicates that the crystals in the PILP samples are of submicroscopic dimensions and lack long-range order. In addition, the broad mineral diffraction peaks indicate that the PILP crystals are stressed nonuniformly (41), which supports the notion that crystal growth occurs between collagen molecules. This result is consistent with the SEM images, taken during this initial phase, in which the mineral does not form rhombohedral crystals but adopts a disk-like shape oriented perpendicular to the long axis of the collagen fibers.

In the second phase, between days 6 and 13, MRM properties appear to plateau, possibly because amorphous calcium carbonate droplets begin to coalesce within the intrafibrillar space of collagen. The formation of a continuous PILP phase within the intrafibrillar space should have little effect on the hydration state or T_2 values of the sponge. In those areas where the PILP phase begins to lose water to form mineral crystals, the hydration state of the sponge and the water proton T_2 values are reduced.

In the third and final phase of the PILP process, after day 15, it is thought that the amorphous calcium carbonate in the intrafibrillar space crystallizes. The encapsulation of collagen molecules by mineral crystals would explain the dramatic reduction in the intensity of the collagen x-ray diffraction peaks. The MTR values are increased compared to controls because of an increase in the rigidity of the collagen molecules due to intrafibrillar mineral formation. It is speculated that as mineralization proceeds, the number of hydroxyl groups on the collagen molecules in free exchange with mobile water molecules is reduced when the collagen molecules are encapsulated by mineral, thereby reducing the measured MTR value for a completely mineralized strip. The fact that the MTR values are indistinguishable after day 24 to values obtained at 13 and 15 days supports the notion that many collagen fibers are not completely encapsulated.

In summary, SEM studies confirmed that we were able to reproduce the PILP experiment in our laboratory and established the intrafibrillar mineralization of the collagen fibrils within the sponge. X-ray diffraction data confirmed that the mineral formed in this system was calcite, and that the calcite peaks were somewhat broad compared to those of isolated crystals because of the short-range order of the crystals that form in the intrafibrillar space. The crystallization of mineral in the intrafibrillar spaces is thought to be the basis of the dramatic reduction in the intensity collagen peaks in the x-ray diffraction data at day 15. Finally, the MRM technique was able to detect the appearance of the earliest mineral deposits, and in this model system, in which the collagen content is constant and the intrafibrillar space is mineralized, the MTR parameter yielded a measure of the change in the rigidity of the collagen network. In conclusion, this work supports the use of MRM to gain important insights into the mineralization process in vivo.

The authors thank Matt Olszta and Dr. Laurie Gower for their helpful advice on setting up and running the PILP experiment. The authors also thank Dr. David Eanes for his careful reading of this manuscript and his helpful suggestions.

This work was supported in part by National Institutes of Health grant AR51446 (K.P.).

The opinions and assertions contained herein are the private views of the authors and are not to be construed as official or reflecting the views of the Department of the Army or the Department of Defense, the American Dental Association Foundation, or the National Institute of Standards and Technology.

REFERENCES

1. Eanes, E. D., D. R. Lundy, and G. N. Martin. 1970. X-ray diffraction study of the mineralization of turkey leg tendon. *Calcif. Tissue Res.* 6:239–248.
2. Katz, E. P., and S. Li. 1972. The molecular packing of collagen in mineralized and non-mineralized tissues. *Biochem. Biophys. Res. Commun.* 46:1368–1373.
3. Bonar, L. C., S. Lees, and H. A. Mook. 1985. Neutron diffraction studies of collagen in fully mineralized bone. *J. Mol. Biol.* 181:265–270.
4. Fratzl, P., N. Fratzl-Zelman, and K. Klaushofer. 1993. Collagen packing and mineralization. An x-ray scattering investigation of turkey leg tendon. *Biophys. J.* 64:260–266.
5. Lees, S., and D. W. Hukins. 1992. X-ray diffraction by collagen in the fully mineralized cortical bone of cow tibia. *Bone Miner.* 17:59–63.
6. Lees, S. 1987. Considerations regarding the structure of the mammalian mineralized osteoid from viewpoint of the generalized packing model. *Connect. Tissue Res.* 16:281–303.
7. Landis, W. J., K. J. Hodgens, J. Arena, M. J. Song, and B. F. McEwen. 1996. Structural relations between collagen and mineral in bone as determined by high voltage electron microscopic tomography. *Microsc. Res. Tech.* 33:192–202.
8. Landis, W. J., M. C. Paine, and M. J. Glimcher. 1977. Electron microscopic observations of bone tissue prepared anhydrously in organic solvents. *J. Ultrastruct. Res.* 59:1–30.
9. Weiner, S., and W. Traub. 1992. Bone structure: from angstroms to microns. *FASEB J.* 6:879–885.
10. Ziv, V., I. Sabanay, T. Arad, W. Traub, and S. Weiner. 1996. Transitional structures in lamellar bone. *Microsc. Res. Tech.* 33:203–213.
11. Davis, C. A., H. K. Genant, and J. S. Dunham. 1986. The effects of bone on proton NMR relaxation times of surrounding liquids. *Invest. Radiol.* 21:472–477.
12. Tenner, M. S., M. Spiller, S. H. Koenig, M. P. Valsamis, S. Childress, R. D. Brown 3rd, and S. S. Kasoff. 1995. Calcification can shorten T2, but not T1, at magnetic resonance imaging fields. Results of a relaxometry study of calcified human meningiomas. *Invest. Radiol.* 30: 345–353.
13. Eng, J., T. L. Ceckler, and R. S. Balaban. 1991. Quantitative 1H magnetization transfer imaging in vivo. *Magn. Reson. Med.* 17:304–314.

14. Ceckler, T. L., S. D. Wolff, V. Yip, S. A. Simon, and R. S. Balaban. 1992. Dynamic and chemical factors affecting water proton relaxation by macromolecules. *J. Magn. Reson.* 98:637–645.

15. Gray, M. L., D. Burstein, L. M. Lesperance, and L. Gehrke. 1995. Magnetization transfer in cartilage and its constituent macromolecules. *Magn. Reson. Med.* 34:319–325.

16. Potter, K., J. Butler, W. E. Horton, and R. G. S. Spencer. 2000. Response of engineered cartilage tissue to biochemical agents as studied by proton MRI microscopy. *Arthritis Rheum.* 43:1580–1590.

17. Seo, G. S., J. Aoki, H. Moriya, O. Karakida, S. Sone, H. Hidaka, and T. Katsuyama. 1996. Hyaline cartilage: in vivo and in vitro assessment with magnetization transfer imaging. *Radiology.* 201:525–530.

18. Laurent, D., J. Wasvary, J. Yin, M. Rudin, T. C. Pellas, and E. O'Byrne. 2001. Quantitative and qualitative assessment of articular cartilage in the goat knee with magnetization transfer imaging. *Magn. Reson. Imaging.* 19:1279–1286.

19. Potter, K., W. J. Landis, and R. G. S. Spencer. 2001. Histomorphometry of the embryonic avian growth plate by proton nuclear magnetic resonance microscopy. *J. Bone Miner. Res.* 16:1092–1100.

20. Potter, K., R. D. Leapman, P. J. Basser, and W. J. Landis. 2002. Cartilage calcification studied by proton nuclear magnetic resonance microscopy. *J. Bone Miner. Res.* 17:652–660.

21. Washburn, N. R., M. Weir, P. Anderson, and K. Potter. 2004. Bone formation in polymeric scaffolds evaluated by proton magnetic resonance microscopy and X-ray microtomography. *J. Biomed. Mater. Res.* 67A:738–747.

22. Potter, K., D. E. Sweet, P. Anderson, G. R. Davis, N. Isogai, S. Asamura, H. Kusuhara, and W. J. Landis. 2006. Non-destructive studies of tissue-engineered phalanges by magnetic resonance microscopy and X-ray microtomography. *Bone.* 38:350–358.

23. Lees, S. 2003. Mineralization of type I collagen. *Biophys. J.* 85:204–207.

24. DiMasi, E., T. Liu, M. J. Olszta, and L. B. Gower. 2005. Laser light scattering studies of a polymer-induced liquid-precursor (PILP) process of mineralization. *Proc. Materials Research Society*, Warrendale, PA. K10.16.

25. Olszta, M. J., D. J. Odom, E. P. Douglas, and L. B. Gower. 2003. A new paradigm for biomineral formation: mineralization via an amorphous liquid-phase precursor. *Connect. Tissue Res.* 44:326–334.

26. Olszta, M. J., E. P. Douglas, and L. B. Gower. 2003. Scanning electron microscopic analysis of the mineralization of type I collagen via a polymer-induced liquid-precursor (PILP) process. *Calcif. Tissue Int.* 72:583–591.

27. Olszta, M. J. 2004. A new paradigm for biomineral formation: mineralization via an amorphous liquid-phase precursor process. PhD thesis. University of Florida, Gainesville, FL.

28. Gregory, C. A., W. G. Gunn, A. Peister, and D. J. Prockop. 2004. An Alizarin red-based assay of mineralization by adherent cells in culture: comparison with cetylpyridinium chloride extraction. *Anal. Biochem.* 329:77–84.

29. Lievremont, M., J. Potus, and B. Guillou. 1982. Use of Alizarin red S for histochemical staining of Ca^{2+} in the mouse; some parameters of the chemical reaction in vitro. *Acta Anat. (Basel).* 114:268–280.

30. Hajnal, J. V., C. J. Baudouin, A. Oatridge, I. R. Young, and G. M. Bydder. 1992. Design and implementation of magnetization transfer pulse sequences for clinical use. *J. Comput. Assist. Tomogr.* 16: 7–18.

31. Laing, J. H., J. P. R. O. Orgel, J. Dubochet, A. Al-Amoudi, T. J. Wess, G. J. Cameron, and C. Laurie. 2003. X-ray diffraction of rat tail tendon at ambient and cryo-cooled temperatures—a comparison. *Fiber Diffraction Review.* 11:119–122.

32. Misof, K., G. Rapp, and P. Fratzl. 1997. A new molecular model for collagen elasticity based on synchrotron X-ray scattering evidence. *Biophys. J.* 72:1376–1381.

33. Cheng, X., and L. B. Gower. 2006. Molding mineral within microporous hydrogels by a polymer-induced liquid-precursor (PILP) process. *Biotechnol. Prog.* 22:141–149.

34. Henkelman, R. M., J. F. Watts, and W. Kucharczyk. 1991. High signal intensity in MR images of calcified brain tissue. *Radiology.* 179:199–206.

35. Kucharczyk, W., and R. M. Henkelman. 1994. Visibility of calcium on MR and CT: can MR show calcium that CT cannot? *AJNR Am. J. Neuroradiol.* 15:1145–1148.

36. Kennan, R. P., K. A. Richardson, J. Zhong, M. J. Maryanski, and J. C. Gore. 1996. The effects of cross-link density and chemical exchange on magnetization transfer in polyacrylamide gels. *J. Magn. Reson.* 110: 267–277.

37. Tessier, J. J., N. Dillon, T. A. Carpenter, and L. D. Hall. 1995. Interpretation of magnetization transfer and proton cross-relaxation spectra of biological tissues. *J. Magn. Reson.* 107:138–144.

38. Fishbein, K. W., Y. A. Gluzband, M. Kaku, H. Ambia-Sobhan, S. A. Shapses, M. Yamauchi, and R. G. Spencer. 2007. Effects of formalin fixation and collagen cross-linking on T2 and magnetization transfer in bovine nasal cartilage. *Magn. Reson. Med.* 57:1000–1011.

39. Lees, S. 1998. Interpreting the equatorial diffraction pattern of collagenous tissues in the light of molecular motion. *Biophys. J.* 75:1058–1061.

40. Jenkens, R., and R. L. Snyder. 1996. Specimen preparation. *In* Introduction to X-Ray Powder Diffractometry. John Wiley & Sons, New York. 235–236.

41. Lundy, D. R., and E. D. Eanes. 1973. An x-ray line-broadening study of turkey leg tendon. *Arch. Oral Biol.* 18:813–826.